Thermally and chemically non-equilibrium modelling of Ar-N2-H2 inductively coupled plasmas at reduced pressure

Thermally and chemically non-equilibrium modelling of Ar-N_2-H_2 inductively coupled plasmas at reduced pressure

Yasunori Tanaka

Faculty of Electrical Engineering and Computer Science, Kanazawa University, Kakuma, Kanazawa 920-1192, JAPAN

Abstract

A two-dimensional thermally and chemically non-equilibrium model was developed for Ar-N_2-H_2 inductively coupled plasmas (ICP) at reduced pressure. The Ar-N_2-H_2 or Ar-NH_3 plasmas at reduced pressure has been widely used for nitriding processing of materials. Totally 164 reactions including 82 forward reactions and their backward reactions were taken into account. Spatial particle composition distribution in the plasma torch as well as in the reaction chamber was derived by solving simultaneously the mass conservation equation of each particle, considering diffusion, convection and production terms.

Key words: Induction thermal plasmas, Chemically non-equilibrium, Thermally non-equilibrium, Reaction rate, High pressure

1. Introduction

Inductively coupled thermal plasmas (ICTPs) have been widely used in various technological fields such as plasma materials processing, plasma waste destruction, plasma spray coatings, etc [1]–[7]. This is because ICTPs have some advantages of high temperature and high enthalpy, and then high reaction activity [8]. In the plasma materials processing field, it is becoming crucial to understand not only the gas flow and temperature fields, but also what chemical reactions happen and dominate chemical fields in the ICTP. It is also essential to understand spatial distribution of chemical species such

as active radicals in the ICTP. Numerical simulation is a powerful tool for this purpose.

Numerical modelling of high power-density inductively coupled plasmas has been done by many researchers to derive the gas flow and temperature fields in plasmas on the assumption of a local thermal equilibrium (LTE) condition [9]–[11]. This LTE model is useful to study transport phenomena of mass, momentum, and energy as well as the gas flow and temperature fields in the high power-density plasmas. However, many conventional LTE models cannot always predict precise chemical fields and particle density distributions in plasmas. This unpredictability is attributed to the fact that these conventional LTE models dictate an infinite reaction rate for any reaction, no diffusion and no convection effects for density distribution of any chemical species, and also force the same electron temperature to the heavy-particle temperature. In contrast to this LTE assumption, high gas flow velocity, rapid state-change, or application of a high electric field, for example, can be seen in actual situations of plasmas. These situations can lead plasmas or a part of plasmas to be under a non-LTE condition.

Until now, several type of non-equilibrium models have been developed even for high-pressure high-power plasmas. For example, Zhao et al. have developed a simple one-temperature chemical non-equilibrium model for a high-power Ar ICP with $SiCl_4$ injection [12]. They accounted for reaction rates of $SiCl_4$ dissociation to predict density fields of chemical species. Some two-temperature models for a pure high-pressure high-power Ar plasma near thermal equilibrium condition, including the ICP, have been developed by some researchers [13, 14, 15]. In this model, electron temperature was solved separately from heavy-particle temperature. The author first developed a two-dimensional two-temperature and chemically non-equilibrium (2T-NCE; Two-Temperature Non-CE) model for high power Ar induction thermal plasmas with nitrogen molecules N_2 [16], and also a time-dependent 2T-NCE model for Ar-N_2 pulse-modulated induction thermal plasmas (PMITP) [17]. Such a two-temperature chemically non-equilibrium model has also been developed recently for Ar-O_2 induction thermal plasmas by Watanabe et al.[18], and for Ar-H_2 induction thermal plasmas by Ye et al. [19]. Recently, a two-temperature chemically non-equilibrium model of Ar-N_2-O_2 supersonic induction thermal plasma has been developed by Morsli et al. [20]. From these calculations, we found thermally and chemically non-equilibrium effects even on high-pressure high-power thermal plasma fields.

On the other hand, actual nitridation processings have been made with

H_2 or NH_3 as an additional gas to enhance nitriding rate [21]. In this case, the existence of radicals like NH is considered to promote the nitriding rate of the metallic surface [21]. Thus, it is important to understand effect of H_2 inclusion on Ar-N_2 plasmas considering reaction rates, convection and diffusion effects for materials nitriding processings. However, use of two kinds of molecular gas mixture causes the plasma composition very complex, which makes it difficult to predict two-temperature fields and chemical species fields.

In this paper, the author developed a two-dimensional two-temperature and chemical non-equilibrium (2T-NCE) model for a tens-kW Ar-N_2 ICP with H_2 at reduced pressure. In this model, 14 species were taken into account, and totally 164 reactions including 82 forward reactions and their backward reactions among the specified species were accounted for. Mass conservation equations for each of species were solved to obtain spatial distributions of each of chemical species. The H_2 inclusion effects and non-equilibrium effects were investigated from the obtained temperature distributions, mass fraction distribution of each of species. Deviation from equilibrium condition was also investigated by comparing temperature field and chemical species fields.

2. Modelling of Ar-N_2-H_2 ICP

2.1. Equilibrium composition of Ar-N_2-H_2 plasmas

For modelling of Ar-N_2-H_2 thermal plasmas, it is useful to consider which species are dominant in equilibrium condition in thermal plasmas. The author considered all the species formed by N and H atoms in the JANAF thermochemical tables[22]: NH, N_3, N_2, N_2H_4, N_2H_2, NH_3, NH_2, H_2, H, N, NH^+, N_2^+, N_2^-, H_2^+, H^+, H^-, N^+, N^{2+}, N^-. In addition, Ar, Ar^+, Ar^{2+}, Ar^{3+} and the electron were taken into account in the calculation. The temperature range for this calculation was set to 300–30000 K in which the conventional thermal plasma is sustained. For a system including these species, the equilibrium composition was calculated by minimization of Gibbs' free energy G of the system:

$$G = \sum_j y_j \left[\mu_j^0 + R_{\mathrm{un}} T \ln \left(\frac{y_j}{\sum_s y_s} \right) + R_{\mathrm{un}} T \ln \left(\frac{P}{P_0} \right) \right] \tag{1}$$

$$\mu_j^0 = -R_{\mathrm{un}} T \ln \left[\left(\frac{2\pi m_j kT}{h^2} \right)^{\frac{3}{2}} Z_j^{\mathrm{int}} \frac{kT}{P_0} \right] + \Delta H_j \tag{2}$$

where y_j is the mole number of species j, $R_{\rm un}$ the universal gas constant, T the temperature, μ_j^0 the chemical potential, m_j the mass of species j, $Z_j^{\rm int}$ the internal partition function, k the Boltzmann constant, h the Planck constant, ΔH_j the standard enthalpy of formation for species j.

Figure 1 shows the equilibrium composition of 98%Ar-1%N_2-1%H_2 thermal plasmas at a pressure of 31 kPa. This pressure is similar to that in our experiment for surface nitridation processing. At 300 K, N_2, H_2 and NH_3 are dominant except Ar atom. As the temperature increases from 300 to 1000 K, significant dissociations of NH_3 occurs. A further increase in temperature from 1000 to 2000 K causes dissociation of H_2 to produce H atoms. On the other hand, N_2 is dissociated by a temperature increase from 2000 to 5000 K, and then N atoms are produced. The molecule NH is considered to one of the important species for surface modification processing [21]. However, the density of NH reaches to only 10^{16} m^{-3} from 3000 to 9000 K. From 4000 to 10000 K, Ar is ionized to produce Ar^+ and electrons.

From this calculation, the author decided the following species to be considered in the plasma fluid modelling: N_2, N_2^+, N, N^+, H_2, H_2^+, H, H^+, NH_3, NH_2, NH, Ar, Ar^+, and the electron.

2.2. Assumptions

In the present modelling work, the followings were assumed [16] : (i) Each of species has the Maxwell-Boltzmann velocity distribution function. (ii) Heavy particles have the same temperature for each of species, that is, the heavy-particle temperature $T_{\rm h}$. The electron is allowed to have a different temperature from the heavy-particle temperature. (iii) The plasma has an axis-symmetric structure. (iv) The plasma is in optically thin. (v) The kinetic energy of electrons is partially transferred to heavy particles through elastic collisions with heavy particles. In addition, electrons lose their kinetic energy through ionization and dissociation reactions with heavy particles. However, the electronic, vibrational and rotational excitations are neglected for simplicity in this model, which mainly involves the energy loss of electrons. This neglect produces overestimation of the electron temperature. (vi) The reaction rates depend on electron temperature $T_{\rm e}$ and/or heavy particle temperature $T_{\rm h}$, not directly on electric field strength. However, in actual situation, electron impact reactions occur in high electric field and low electron density situation near the plasma torch region, whose reaction rates depend strongly on electric field. The present model may cause lower dissociation of molecules, for example. (vii) There are only 14 kinds of

species: N_2, N_2^+, N, N^+, H_2, H_2^+, H, H^+, NH_3, NH_2, NH, Ar, Ar^+, and the electron.

2.3. Governing equations

According to the assumptions introduced in the previous section, the plasma is governed by the following equations described in Tab. 1. These are similar to those in our previous work for Ar-N_2 ICP[16]. In this table, Eq.(1) is the mass conservation equation of plasmas, Eqs.(2),(3) and (4) indicates the momentum conservation equations for axial, radial and swirl direction components, respectively, Eq.(5) is the translational energy conservation equation for heavy particles, Eq.(6) is the energy conservation equation for electrons, Eq.(7) is the mass conservation equation for species j, Eq.(8) shows the Maxwell equations for electromagnetic fields in terms of vector potential. Eqs.(9) and (10) are the relationship between electromagnetic field and vector potential, Eq.(11) indicates the reaction heat per unit volume and second, Eq.(12) is the translational enthalpy for heavy particles, Eq.(13) is the energy transfer through elastic collision between electrons and heavy particles, Eq.(14) is the relative velocity between electrons and heavy particles, Eq.(15) is the relation between density n_j and mass fraction Y_j for species j, Eq.(16) is the equation of state. Eq.(17) means the quasi-neutrality, Eq.(18) corresponds to the balance of sum of mass fractions. Eq.(19) expresses the effective diffusion coefficient of species j, Eq.(20) is the electrical conductivity, Eq.(21) is the viscosity, Eq.(22) is the translational thermal conductivity of heavy particles, Eq.(23) is the translational thermal conductivity of electrons. Thermodynamic and transport properties of thermal plasmas were calculated at each position using the derived local particle composition, electron temperature and heavy particle temperature. Transport properties were calculated by the first order approximation of Chapman-Enskog method using the collision cross section data. The first order approximation of Chapman-Enskog method is roughly enough for calculating transport properties of thermal plasma at temperatures below 10000 K[16].

2.4. Reactions

The selection of the reactions were related to the validity of the calculation. We carefully choose possible reactions between 14 kinds of species with reaction rates obtained. The reaction rates affect accuracy of the calculation. Table 2 summarizes the reactions taken into account in the present calculation. For the considered 14 kinds of species, the author considered

164 reactions including 82 forward reactions and their backward reactions in this table. Note that 'M' in the table indicates all the heavy particles taken into account. The reaction rates for the reactions in Tab. 2 were obtained in [23]–[27], etc.

2.5. Calculation condition and boundary condition

Figure 2 depicts the cross section of the plasma torch treated here. This plasma torch is composed of two-axial quartz tubes. The inner quartz tube has an inner diameter of 70 mm and a length of 330 mm. Between the two quartz tubes, cooling water flows to keep the wall temperature 300 K. Downstream of the plasma torch, the reaction chamber made of SUS304 is installed, whose wall is cooled by flowing water. On the other hand, an 8-turn induction coil is wound around the plasma torch. Its length is 150 mm. Gas is supplied along the inner wall of the inner quartz tube as a sheath gas. For the calculation, the gas flow rate is set to 98/1.0/1.0 slpm for $Ar/N_2/H_2$. The swirl angle was set to 30°. The pressure is fixed at 31 kPa(=230 torr).

The calculation space was set to z-r cylindrical space shown in Fig.2. This space was divided into 92×66 cells. Heat transfer between the plasma and the wall was considered as a boundary condition for energy conservation of heavy particles. The gas flow velocity was set to 0 m/s at all the wall. The temperature of injected gas was set to T_h=T_e =300 K. At z=910 mm, the gas was set to flow out without gradient. Input power was fixed at 13.5 kW.

The calculation validity in absolute value depends mainly on cross section used, the selected reactions, the reaction rates. However, in this paper we paid attention especially to difference between the one-temperature chemically equilibrium 1T-CE model and two-temperature chemically non-equilibrium (2T-NCE) model. This comparison can be done because both models used the same data in transport properties calculation, and then the reaction rate effects in non-equilibrium state can be embossed.

3. Results and discussions

3.1. Temperature distribution

3.1.1. Difference between electron and heavy-particle temperatures

Figure 3 indicates the two-dimensional distribution of T_e and T_h of 98%Ar-1%N_2-1%H_2 thermal plasmas calculated by the present 2T-NCE model. For comparison, the temperature distribution calculated by the LTE model, i.e. a

conventional one-temperature chemical equilibriums (1T-CE) model was also shown in Fig. 4. From Fig. 3, both the electron temperature T_e and the heavy particle temperature T_h reach up to 9000 K in the plasma torch. In addition, T_e is higher than T_h around the wall of the plasma torch, i.e. around radial position of $20< r <35$ mm. On the other hand, T_h has a higher peak value around a point (z, r)=(155 mm, 17mm) than T_e. The comparison between T_e and T_h can easily be made in Fig. 5, which represents the radial distributions of T_e and T_h at an axial position of 155 mm, i.e. at mid-coil position, predicted by the 2T-NCE model. This figure also includes the radial distribution of temperature T by the 1T-CE model. From this figure, we can find that there is a large deviation between T_e and T_h around the torch wall. This deviation is attributed to higher electric field strength and lower collision frequency between electrons and heavy particles near the wall. On the other hand, at $0< r <17$ mm, T_e is a little lower than T_h. This lower T_e is considered to arise from the radiation loss from electrons and energy loss for ionization, meanwhile the heavy particles are heated mainly by the radial convection and dissociative recombination reactions. Such energy conservations for electrons and heavy particles for determining T_e and T_h will be discussed in later section. It is also seen from Figs. 3 and 4 and also Fig. 5 that T_h calculated by the 2T-NCE model is similar to T by the 1T-CE model. These results mean that the 1T-CE model, i.e. the LTE model can predict T_h in this case, but it is difficult to predict T_e which dominates some electron-related reactions including electron impact ionization reactions.

3.1.2. Effect of H_2 inclusion

Effect of H_2 inclusion on the temperature can be also studied using the 2T-NCE model by comparing the temperature distribution of a 98%Ar-1%N_2-1%H_2 plasma and that of a 98%Ar-2%N_2 plasma. Figure 6 shows the temperature distribution of a 98%Ar-2%N_2 thermal plasma without H_2 inclusion by the 2T-NCE model. Comparison between Figs. 3 and 6 indicates clearly that H_2 inclusion causes a marked shrinkage of both high T_e region and high T_h region in a Ar-N_2 plasma in the plasma torch as well as in the reaction chamber. Especially, in the plasma torch region, such a shrinkage is more effective. Figure 7 represents the radial temperature distribution of the 98%Ar-2%N_2 thermal plasma at an axial position of 155 mm, i.e at mid coil region for easy comparison with the radial temperature distribution of the 98%Ar-1%N_2-1%H_2 plasma indicated in Fig. 5. The shrinkage of high temperature region for T_e and T_h can be seen apparently in the 98%Ar-1%N_2-1%H_2 plasma com-

pared with the 98%Ar-2%N_2 plasma. This shrinkage of high temperature regions is mainly due to dissociation of H_2. The dissociation energy for H_2 is only 4.478 eV while that for N_2 is 9.759 eV. Thus, H_2 is more easily dissociated by collisions with heavy particles than N_2. It is noted, however, that the present calculation does not take into account electron impact dissociations of N_2 and H_2 because these molecules are present mainly in low temperature region whereas electrons are mostly in high temperature region. In actual situation, electron may exist near the torch wall due to ambipolar diffusion, where N_2 and H_2 are present and high electric field strength is applied to electrons, as seen in later section. In this situation, the electron impact with molecules may affect dissociation degree of molecules. This phenomenon would be taken into account in future work.

3.1.3. Energy balance

Electron temperature and heavy particle temperature are determined by energy balance for each of species. Each of terms in electron energy conservation equations were separately calculated to obtain energy balance for electrons. Figure 8 shows the calculated energy terms in the energy conservation equation for electrons in a Ar-1%N_2-1%H_2 plasma at axial position of 155 mm. In this figure, $\sigma|E_\theta|^2$ indicates the joule heating term, the quantity $-E_{\rm eh}$ is the energy transfer term between electrons to heavy particles, $-P_{\rm rad}$ is the radiation loss term, $-\Sigma\Delta Q_\ell$ means the reaction heat term for electrons, 'R-cond.' is the radial conduction term, $-{\rm div}(h_{\rm e}\Gamma_{\rm e})$ is the enthalpy flow term due to diffusion. Electrons receive energy if the value of each term is positive. On the other hand, electrons loses their energy if it is negative. From this figure, electrons are mainly heated by joule heating $\sigma|E_\theta|^2$ at $r < 30$ mm, whereas they lose energy by reactions, especially ionization reactions of N atom N + e $\rightarrow$ N^+ + 2e at r <22 mm. Electrons lose energy through elastic collisions with heavy particles to heat those heavy particles at 18< r <22 mm. Meanwhile, electrons are rather heated by collisions with hot heavy particles, which is heated by dissociative recombination reactions N_2^+ + e $\rightarrow$ 2N.

Figure 9 depicts the calculated energy terms in the energy conservation equation for heavy particles in a Ar-1%N_2-1%H_2 plasma at axial position of 155 mm. From this figure, we can see dominant terms to determine heavy particle temperature $T_{\rm h}$. The quantity 'R-conv.' indicates the radial convection term, 'Z-conv.' means the axial convection term, 'R-cond.' is the radial conduction term, $E_{\rm eh}$ is the energy transfer term between electrons and heavy

particles, and $-\Sigma\Delta Q_\ell$ is the reaction heat terms for heavy particles. Heavy particles around the torch axis are heated mainly by the radial convection because the gas heated at $10 < r < 22$ mm flows in the radial direction onto the torch axis. Then, that heated heavy particles flow in the axial direction near the torch axis, which plays an role of energy loss for heavy particles there. On the other hand, heavy particles at $18< r < 22$ mm receive energy through elastic collisions with electrons heated by joule heating. However, heavy particles at $r < 18$ mm rather give energy to electrons. Heavy particles at $r < 18$ mm receive energy mainly due to dissociative recombination reactions $N_2^+ + e \rightarrow 2N$, as described previously. This reaction releases energy 9.65 eV to give translational energy of N atoms.

3.2. Spatial distribution of mass fraction of each species

It is pointed out that nitrogen atomic density is one of the crucial factors for surface nitriding process[21]. Figure 10 shows the mass fraction distributions of N_2 and N in 98%Ar-1%N_2-1%H_2 plasma calculated by the 2T-NCE model. Contours are plotted in logarithm scale. The N_2 mass fraction Y_{N_2} is smaller in high temperature area in the plasma torch because of N_2 dissociation. The N mass fraction Y_N is also smaller in this area because of N ionization. For downstream of the plasma torch, i.e. $200 < z < 250$ mm, Y_N reaches more than 10^{-2}. Further downstream region, Y_N is markedly decayed in the reaction chamber, because of N atom association reaction there.

It is also considered that radicals such as NH and NH_2 may enhance the nitriding rate of metallic surface processings [21]. Thus, it is important to understand mass fraction distributions of them. Figure 11 shows the mass fraction distribution of NH_2 and NH in Ar-N_2-H_2 plasma calculated by the 2T-NCE model. The NH_2 mass fraction is relatively small with less than 10^{-9}, and NH_2 exists away from the axissymmetric axis of the torch. On the other hand, NH radicals exist mainly around the axissymmetric axis with mass fractions of more than 10^{-7} in wide area, i.e., both in the plasma torch and the reaction chamber downstream of the torch.

For comparison, mass fraction distributions of N_2 and N in 98%Ar-1%N_2-1%H_2 plasma by the 1T-CE model were plotted in Fig. 12. The mass fraction distributions of N_2 and N by the 2T-NCE model has roughly similar tendency to those by the 1T-CE model. However, the magnitudes of mass fraction is different between results by these two models especially in the plasma torch region. For example, N_2 mass fraction is smaller in high temperature region calculated by the 1T-CE model than that by the 2T-NCE model. Figure 13

shows the radial distributions of particle composition at an axial position of 155 mm in Ar-N_2-H_2 plasmas by the 2T-NCE and 1T-CE models. Generally, similar composition can be found. Nevertheless, NH_3 exists near the wall for the calculation result by the 1T-CE model, while NH_3 density is lower than 10^{17} m^{-3} in the result by the 2T-NCE model. The dissociation degree of N_2, and then N_2 and N densities by the 1T-CE is markedly different from those predicted by the 2T-NCE model. For example, on the center axis, N_2 and N densities are respectively 3.92×10^{19} m^{-3} and 2.53×10^{21} m^{-3} predicated by the 1T-CE model. These values are about 10 times higher than those calculated by the 2T-NCE model, which are 2.03×10^{20} and 7.26×10^{21} m^{-3} for N_2 and N densities. In addition, the electron density near the wall is much higher by the 2T-NCE model than that by the 1T-CE model. For example, at r=24.5 mm, the electron density is 4.07×10^{19} m^{-3} predicted by the 2T-NCE model, while the electron density is predicted to be 2.39×10^{14} m^{-3} by the 1T-CE model. Electrons and H ions are transported strongly in radial direction by ambipolar diffusion, because H ion has its light mass. These deviations in particle composition depend mainly on reaction rates used in the 2T-NCE model.

4. Summary

In this paper, a model of high-power Ar-N_2-H_2 induction thermal plasmas is developed, in which deviation between electron temperature and heavy particle temperature and chemically non-equilibrium effects were taken into account. It was found that inclusion of H_2 causes a marked shrinkage of high temperature region both for electron temperature and heavy particle temperature in Ar-N_2 plasmas. Electron temperature is determined mainly by joule heating, ionization reactions, energy transfer between electron and heavy particles, meanwhile heavy particle temperature is done by dissociative recombination reactions and convection effects. Chemical species distributions were predicted by the developed model considering reaction rate, convection and diffusion effects. It was found that composition was influenced by reaction rates which causes chemically non-equilibrium effects.

References

[1] Y.K.Chae, H.Ohno, K.Eguchi, and T.Yoshida, Ultrafast deposition of microcrystalline Si by thermal plasma chemical vapor deposition *J.Appl.Phys.*, **89**, 8311–8315, 2001

[2] S.Son, M.Taheri, E.Carpenter, V.G.Harris, and M.E.McHenry, Synthesis of ferrite and nickel ferrite nanoparticles using radio-frequency thermal plasma torch *J.Appl.Phys.*, **91**, 7589–7591,2002

[3] Y.Tanaka and T.Sakuta, Investigation on plasma-quenching efficiency of various gases using the inductively coupled thermal plasma technique: effect of various gas injection on Ar thermal ICP, *J.Phys.D:App.Phys.*, **35**, 2149–2158, 2002

[4] F.Bourg, S.Pellerin, D.Morvan, J.Amouroux, and J.Chapelle, Spectroscopic diagnostic of an argon-hydrogen RF inductive thermal plasma torch at atmospheric pressure used for silicon hydrogenation *J.Phys.D:Appl.Phys.*, **35**, 2281–2290, 2002

[5] C.Wang, A.Inazaki, T.Shirai, Y.Tanaka, T.Sakuta, H.Takikawa, and H.Matsuo, Effect of ambient gas and pressure on fullerene systhesis in induction thermal plasma *Thin Solid Film*, **425**, 42–49, 2003

[6] I. Mohai, Reduction of metallurgical wastes in an rf thermal plasma reactor, *Plasma Chem. Plasma Process.*, **21**, 547–563, 2001

[7] R. Guddeti, Depolymerization of polyethylene using induction-coupled plasma technology, *Plasma Chem. Plasma Process.*, **20**, 37–64, 2000.

[8] M. Boulos, P. Fauchais and E. Pfender, *Thermal Plasmas Fundamentals and Applications*, vol.I pp.33–43, 1994, Plenm Press New York

[9] S. Xue, P. Proulx and M. I. Boulos, Three dimensional coil effects in inductive plasma flow modelling, *Proc. Int. Symp. on Plasma Chem.* vol III, pp.1221–126, 2001

[10] S. Xue, P.Proulx and M. I. Boulos, Extended-field electromagnetic model for inductively coupled plasma *J.Phys. D: Appl. Phys.* **34** 1897–1906, 2001

[11] D.Bernardi, V.Colombo, E.Ghedini, and A.Mentrelli, Three-dimensional modelling of inductively coupled plasma torches, *Proc. Int. Symp. on Plasma Chem.* Inv3 p.138 in Abstracts, ISPC-635 in CD-ROM, 2003

[12] G.Y.Zhao, J.Mostaghimi and M.I.Boulos, The induction plasma chemical reactor: Part II. Kinetic model *Plasma Chem. Plasma Process.*, **10**, 151–166, 1990

[13] J.Mostaghimi, P.Proulx and M.I.Boulos, A two-temperature model of the inductively coupled rf plasma *J.Appl.Phys.* **61** 1753–1760, 1987

[14] S.H.Paik and E.Pfender, Modeling of an inductively coupled plasma at reduced pressures, *Plasma Chem. Plasma Process.*, **10**, 167–188, 1990

[15] Y.Bartosiewicz, P.Proulx and Y.Mercadier, A self-consistent two-temperature model for the computation of supersonic argon plasma jets, *J.Phys.D:Appl.Phys.*, **35**, 2139–2148, 2003

[16] Y.Tanaka, Two-temperature chemically non-equilibrium modelling of high-power Ar-N_2 inductively coupled plasmas at atmospheric pressure, *J.Phys.D:Appl.Phys.*, **37**, 1190–1205, 2004

[17] Y.Tanaka, Time-dependent two-temperature chemically non-equilibrium modelling of high-power Ar-N_2 pulse-modulated inductively coupled plasmas at atmospheric pressure, *J.Phys.D:Appl.Phys.*, **39**, 307–319, 2006

[18] T. Watanabe, N.Atsuchi, and M. Shigeta, Two-temperature chemically non-equilibrium modeling of argon induction plasmas with diatomic gases, *Int. J. Heat and Mass Transfer*, **49** (25-26), 4867–4876, 2006

[19] R. Ye, A.B.Murphy, T.Ishigaki, Numerical modeling of an Ar-H_2 radio-frequency plasma reactor under thermal and chemical nonequilibrium conditions, *Plasma Chem. & Plasma Process.*, **27**, 189–204, 2007

[20] M. E. Morsli and P. Proulx, Two-temperature chemically non-equilibrium modelling of an air supersonic ICP, *J. Phys. D: Appl. Phys.*, **40**, 4810–4828, 2007.

[21] M.Tamaki, Y.Tomii, N.Yamamoto, The role of hydrogen in plasma nitriding: Hydrogen behavior in the titanium nitride layer, *Plasma & Ions*, **3**, 33-39, 2000.

[22] M. W. Chase, Jr. et al, *JANAF Thermochemical Tables Thrid Edition*, *J.Phys.Chem.Ref.Data*, **14**, Supp.No.1, 1985 NIST

[23] M.G.Dunn and K.A.Lordi, Measurement of $N_2^+ + e^-$ dissociative recombination in expanding nitrogen flows *AIAA*, **8**, 339–345, 1970

[24] T.G.Owano, C.H.Kruger and Beddini 1993 Electron-ion three-body recombination coefficient of argon *AIAA*, **31**, 75–82, 1993

[25] T.Takagi, et al, *Analysis of Complex Flows* 1995, University of Tokyo Press.

[26] Chemical Kinetics, NIST Scientific and Technical Database +`http://www.nist.gov/srd/chemkin.htm`+

[27] A.V. Phelps, Cross sections and swarm coefficients for nitrogen ions and neutrals in N_2 and argon ions and neutrals in Ar for energies from 0.1 eV to 10 keV, *J. Phys. Chem. Ref. Data*, **20**, 557–573, 1991

List of table captions

List of figure captions

Table 1: Governing equations used in the present paper.

Mass conservation:

$$\frac{\partial \rho}{\partial t} + \frac{\partial (\rho u)}{\partial z} + \frac{1}{r}\frac{\partial (r\rho v)}{\partial r} = 0 \tag{1}$$

Momentum conservation:

$$\begin{aligned}
&\frac{\partial (\rho u)}{\partial t} + \frac{\partial (u\rho u)}{\partial z} + \frac{1}{r}\frac{\partial (rv\rho u)}{\partial r} \\
&= -\frac{\partial p}{\partial z} + 2\frac{\partial}{\partial z}\left(\eta \frac{\partial u}{\partial z}\right) \\
&+ \frac{1}{r}\frac{\partial}{\partial r}\left[\eta r\left(\frac{\partial u}{\partial r} + \frac{\partial v}{\partial z}\right)\right] + \mu_0 \sigma \Re[\dot{E}_\theta \bar{H}_r^*]
\end{aligned} \tag{2}$$

$$\begin{aligned}
&\frac{\partial (\rho v)}{\partial t} + \frac{\partial (u\rho v)}{\partial z} + \frac{1}{r}\frac{\partial (rv\rho v)}{\partial r} \\
&= -\frac{\partial p}{\partial r} + \frac{\partial}{\partial z}\left[\eta\left(\frac{\partial v}{\partial z} + \frac{\partial u}{\partial r}\right)\right] \\
&+ \frac{2}{r}\frac{\partial}{\partial r}\left(\eta r \frac{\partial v}{\partial r}\right) - 2\eta\frac{v}{r^2} + \mu_0 \sigma \Re[\dot{E}_\theta \bar{H}_z^*]
\end{aligned} \tag{3}$$

$$\begin{aligned}
&\frac{\partial (\rho w)}{\partial t} + \frac{\partial (u\rho w)}{\partial z} + \frac{1}{r}\frac{\partial (rv\rho w)}{\partial r} \\
&= \frac{\partial}{\partial z}\left(\eta \frac{\partial w}{\partial z}\right) + \frac{1}{r}\frac{\partial}{\partial r}\left(r\eta \frac{\partial w}{\partial r}\right) - \frac{\rho v w}{r} - \frac{w}{r}\frac{\partial}{\partial r}(r\eta)
\end{aligned} \tag{4}$$

Translational energy conservation of heavy particle:

$$\begin{aligned}
&\frac{\partial (\rho h')}{\partial t} + \frac{\partial (u\rho h')}{\partial z} + \frac{1}{r}\frac{\partial (rv\rho h')}{\partial r} \\
&= \frac{\partial}{\partial z}\left(\lambda_{\mathrm{h}}^{\mathrm{tr}} \frac{\partial T_{\mathrm{h}}}{\partial z}\right) + \frac{1}{r}\frac{\partial}{\partial r}\left(r\lambda_{\mathrm{h}}^{\mathrm{tr}} \frac{\partial T_{\mathrm{h}}}{\partial r}\right) \\
&+ \sum_{j\ (j\neq \mathrm{e})}^{N}\left[\frac{\partial}{\partial z}\left(\rho D_j' h_j' \frac{\partial Y_j}{\partial z}\right) + \frac{1}{r}\frac{\partial}{\partial r}\left(r\rho D_j' h_j' \frac{\partial Y_j}{\partial r}\right)\right] \\
&- \sum_{\ell\ (\beta_{\mathrm{e}\ell}^{\mathrm{f}} - \beta_{\mathrm{e}\ell}^{\mathrm{r}} = 0)}^{L} \Delta Q_\ell + E_{\mathrm{eh}}
\end{aligned} \tag{5}$$

Energy conservation of electron:

$$\begin{aligned}
&\frac{\partial}{\partial t}\left(n_{\mathrm{e}}\frac{5}{2}\kappa T_{\mathrm{e}}\right) + \frac{\partial}{\partial z}\left(u n_{\mathrm{e}}\frac{5}{2}\kappa T_{\mathrm{e}}\right) + \frac{1}{r}\frac{\partial}{\partial r}\left(rv n_{\mathrm{e}}\frac{5}{2}\kappa T_{\mathrm{e}}\right) \\
&= \frac{\partial}{\partial z}\left(\lambda_{\mathrm{e}}^{\mathrm{tr}} \frac{\partial T_{\mathrm{e}}}{\partial z}\right) + \frac{1}{r}\frac{\partial}{\partial r}\left(r\lambda_{\mathrm{e}}^{\mathrm{tr}} \frac{\partial T_{\mathrm{e}}}{\partial r}\right) \\
&- \frac{\partial}{\partial z}\left(\frac{1}{m_{\mathrm{e}}}\frac{5}{2}\kappa T_{\mathrm{e}}\Gamma_{\mathrm{e}z}\right) - \frac{1}{r}\frac{\partial}{\partial r}\left(r\frac{1}{m_{\mathrm{e}}}\frac{5}{2}\kappa T_{\mathrm{e}}\Gamma_{\mathrm{e}r}\right) \\
&- \sum_{\ell\ (\beta_{\mathrm{e}\ell}^{\mathrm{f}} - \beta_{\mathrm{e}\ell}^{\mathrm{r}} \neq 0)}^{L} \Delta Q_\ell + \sigma \dot{E}_\theta \bar{E}_\theta^* - P_{\mathrm{rad}} - E_{\mathrm{eh}}
\end{aligned} \tag{6}$$

Mass conservation of species j:

$$\begin{aligned}
&\frac{\partial (\rho Y_j)}{\partial t} + \frac{\partial (u\rho Y_j)}{\partial z} + \frac{1}{r}\frac{\partial (rv\rho Y_j)}{\partial r} \\
&= \frac{\partial}{\partial z}\left(\rho D_j' \frac{\partial Y_j}{\partial z}\right) + \frac{1}{r}\frac{\partial}{\partial r}\left(r\rho D_j' \frac{\partial Y_j}{\partial r}\right) \\
&+ m_j \sum_{\ell=1}^{L}(\beta_{j\ell}^{\mathrm{r}} - \beta_{j\ell}^{\mathrm{f}})\left(\alpha_\ell^{\mathrm{f}}\prod_{i=1}^{N} n_i^{\beta_{i\ell}^{\mathrm{f}}} - \alpha_\ell^{\mathrm{r}}\prod_{i=1}^{N} n_i^{\beta_{i\ell}^{\mathrm{r}}}\right)
\end{aligned} \tag{7}$$

Maxwell equation by vector potential:

$$\frac{\partial^2 \dot{A}_\theta}{\partial z^2} + \frac{1}{r}\frac{\partial}{\partial r}\left(r\frac{\partial \dot{A}_\theta}{\partial r}\right) - \frac{\dot{A}_\theta}{r^2} = \bar{i}\mu_0 \sigma \omega \dot{A}_\theta \tag{8}$$

$$H_z = \frac{1}{\mu_0}\frac{1}{r}\frac{\partial}{\partial r}(r\dot{A}_\theta), \quad H_r = -\frac{1}{\mu_0}\frac{\partial \dot{A}_\theta}{\partial z} \tag{9}$$

$$\dot{E}_\theta = -\bar{i}\omega \dot{A}_\theta \tag{10}$$

Reaction heat per unit volume and time:

$$\Delta Q_\ell = \psi_{\mathrm{reac}\ell}\left(\alpha_\ell^{\mathrm{f}}\prod_{i=1}^{N} n_i^{\beta_{i\ell}^{\mathrm{f}}} - \alpha_\ell^{\mathrm{r}}\prod_{i=1}^{N} n_i^{\beta_{i\ell}^{\mathrm{r}}}\right) \tag{11}$$

Translational enthalpy of heavy particles:

$$h' = \sum_{j\neq \mathrm{e}} Y_j h_j', \qquad h_j' = \frac{1}{m_j}\left(\frac{5}{2}kT_{\mathrm{h}}\right) \tag{12}$$

Energy transfer from electron to heavy particles:

$$E_{\mathrm{eh}} = \sum_{j\neq \mathrm{e}} \frac{3}{2}\kappa(T_{\mathrm{e}} - T_{\mathrm{h}})\frac{2m_j m_{\mathrm{e}}}{(m_j + m_{\mathrm{e}})^2} n_j n_{\mathrm{e}} \pi \bar{\Omega}_{\mathrm{e}j}^{(2,2)} \bar{v}_{\mathrm{e}j} \tag{13}$$

$$\bar{v}_{\mathrm{e}j} = \sqrt{\frac{8\kappa T_{\mathrm{e}}(m_{\mathrm{e}} + m_j)}{\pi m_{\mathrm{e}} m_j}} \tag{14}$$

Relation between mass density and mass fraction:

$$n_j = \frac{\rho Y_j}{m_j} \tag{15}$$

Equation of state:

$$\rho = \frac{p}{\frac{Y_{\mathrm{e}}}{m_{\mathrm{e}}}\kappa T_{\mathrm{e}} + \sum_{j\neq \mathrm{e}}\frac{Y_j}{m_j}\kappa T_{\mathrm{h}}} \tag{16}$$

Quasi-neutrality:

$$\frac{Y_{\mathrm{e}}}{m_{\mathrm{e}}} = \sum_{j(\mathrm{positive-ion})} \frac{Y_j}{m_j} \tag{17}$$

Balance of mass fraction:

$$\sum_j Y_j = 1 \tag{18}$$

Effective diffusion coefficient of heavy particle:

$$D_j' = \frac{1 - Y_j}{\sum_{k\neq j}\frac{x_i p \Delta_{ij}^{(1)}}{\kappa T_{\mathrm{h}}}} \tag{19}$$

Electrical conductivity:

$$\sigma = \frac{e^2}{\kappa T_{\mathrm{e}}}\frac{n_{\mathrm{e}}}{\sum_{j\neq \mathrm{e}} n_j \Delta_{\mathrm{e}j}^{(1)}} \tag{20}$$

Viscosity:

$$\eta = \sum_{j=1}^{N}\frac{m_j n_j}{\sum_{i=1}^{N} n_i \Delta_{ij}^{(2)}} \tag{21}$$

Translational thermal conductivity of heavy particle:

$$\lambda_{\mathrm{h}}^{\mathrm{tr}} = \frac{15}{4}\kappa \sum_{i\neq \mathrm{e}}\frac{n_i}{\sum_j \xi_{ij} n_j \Delta_{ij}^{(2)}} \tag{22}$$

Translational thermal conductivity of electron:

$$\lambda_{\mathrm{e}}^{\mathrm{tr}} = \frac{15}{4}\kappa \frac{n_{\mathrm{e}}}{\sum_j \xi_{\mathrm{e}j} n_j \Delta_{\mathrm{e}j}^{(2)}} \tag{23}$$

$$\frac{1}{\Delta_{ij}^{(1)}} = \frac{3}{8}\sqrt{\frac{\pi\kappa T_{\mathrm{h,e}}(m_i + m_j)}{2m_i m_j}}\frac{1}{\pi \bar{\Omega}_{ij}^{(1,1)}} \tag{24}$$

$$\frac{1}{\Delta_{ij}^{(2)}} = \frac{5}{16}\sqrt{\frac{\pi\kappa T_{\mathrm{h,e}}(m_i + m_j)}{2m_i m_j}}\frac{1}{\pi \bar{\Omega}_{ij}^{(2,2)}} \tag{25}$$

$$\xi_{ij} = 1 + \frac{(1 - m_i/m_j)(0{,}45 - 2{,}54 m_i/m_j)}{(1 + m_i/m_j)^2} \tag{26}$$

where t: time (s), r: radial position (m), z: axial position (m), u: axial flow velocity (m/s), v: radial flow velocity (m/s), ρ: mass density (kg/m^3), p: pressure (Pa), η: viscosity (Pa·s), h': whole enthalpy of heavy particle (J/kg), h_j': enthalpy of species j (J/kg), T_{h}: heavy particle temperature (K), T_{e}: electron temperature (K), $\lambda_{\mathrm{h}}^{\mathrm{tr}}$, $\lambda_{\mathrm{e}}^{\mathrm{tr}}$: translational thermal conductivity of heavy particle and electron, respectivly (W/m/K), σ: electrical conductivity (S/m), P_{rad}: radiation loss (W/m^3), D_j': effective diffusion coefficient of heavy particle j (m^2/s), n_j: number density of species j (m^{-3}), Y_j: mass fraction of species j, x_j: mole fraction of species j, m_j: mass of species j (kg), $\Gamma_{\mathrm{e}r}$, $\Gamma_{\mathrm{e}z}$: radial and axial electron flux due to ambipoler diffusion (1/m^2/s), α_ℓ^{f}, α_ℓ^{r}: rate coefficients of forward and backward reaction ℓ, respectively, $\beta_{j\ell}^{\mathrm{f}}$, $\beta_{j\ell}^{\mathrm{r}}$: stoichiometric number of species j in forward and backward reaction ℓ, μ_0: permeability of vacuum (H/m), κ: Boltzmann constant (J/K), A_θ: vector potential (V·s/m), ω: angular frequency of coil current (rad/s), E_θ: electric field strength (V/m), H_z: axial magnetic field strength (A/m), H_r: radial magnetic field strength (A/m), $\bar{i}$: complex index ($\bar{i}^2 = -1$), $\psi_{\mathrm{reac}\ell}$: reaction heat for reaction ℓ (J), ΔQ_ℓ: reaction heat per unit volume and time (W/m^3), $\pi\bar{\Omega}_{ij}^{(1,1)}$: momentum transfer collision integrals (m^2), $\pi\bar{\Omega}_{ij}^{(2,2)}$: viscosity collision integrals (m^2), $\bar{v}_{\mathrm{e}j}$: relative average velocity between electron and heavy particles (m/s), N: total number of species, L: total number of reactions. E_{eh}: energy transfer between electron and heavy particles (W/m^3).

Table 2: Reactions taken into account in the present calculation.

N°	Reaction			a_ℓ	b_ℓ	c_ℓ	Reaction heat $\psi_{\mathrm{reac}\ell}$ (eV)	Dep.Temp. for forward	Dep.Temp. for backward
1	$N_2 + N_2$	$\rightarrow$	$N + N + N_2$	4.98×10^{-9}	-1.5	113260	9.759	T_h	T_h
2	$N_2 + N$	$\rightarrow$	$N + N + N$	2.49×10^{-8}	-1.5	113260	9.759	T_h	T_h
3	$N_2^+ + N$	$\rightarrow$	$N_2 + N^+$	1.30×10^{-19}	0.5	0	-1.047	T_h	T_h
4	$N_2^+ + e$	$\rightarrow$	$N + N$	2.49×10^{-8}	-1.5	0	-5.821	T_e	T_h
5	$N^+ + e + e$	$\rightarrow$	$N + e$	2.29×10^{-20}	-4.5	0	-14.534	T_e	T_e
6	$N_2^+ + N_2 + e$	$\rightarrow$	$N_2 + N_2$	6.07×10^{-34}	-2.5	0	-15.580	T_e	T_h
7	$N_2^+ + N + e$	$\rightarrow$	$N_2 + N$	1.66×10^{-35}	-2.5	0	-15.580	T_e	T_h
8	$N^+ + N_2 + e$	$\rightarrow$	$N + N_2$	6.07×10^{-34}	-2.5	0	-14.534	T_e	T_h
9	$N^+ + N + e$	$\rightarrow$	$N + N$	1.66×10^{-35}	-2.5	0	-14.534	T_e	T_h
10	$Ar + e$	$\rightarrow$	$Ar^+ + e + e$	-	-	-	15.760	T_e	T_e
11	$Ar + Ar$	$\rightarrow$	$Ar^+ + e + Ar$	-	-	-	15.760	T_h	T_e
12	$N_2 + Ar$	$\rightarrow$	$N + N + Ar$	2.49×10^{-8}	-1.5	113260	9.759	T_h	T_h
13	$N_2 + Ar^+$	$\rightarrow$	$N + N + Ar^+$	2.49×10^{-8}	-1.5	113260	9.759	T_h	T_h
14	$N_2^+ + Ar + e$	$\rightarrow$	$N_2 + Ar$	1.66×10^{-35}	-2.5	0	-15.580	T_e	T_h
15	$N^+ + Ar + e$	$\rightarrow$	$N + Ar$	1.66×10^{-35}	-2.5	0	-14.534	T_e	T_h
16	$H + H + H_2$	$\rightarrow$	$H_2 + H_2$	2.54×10^{-43}	-0.6	0	-4.478	T_h	T_h
17	$H + H + N_2$	$\rightarrow$	$H_2 + N_2$	2.76×10^{-42}	-1.0	0	-4.478	T_h	T_h
18	$H + H + Ar$	$\rightarrow$	$H_2 + Ar$	2.76×10^{-42}	-1.0	0	-4.478	T_h	T_h
19	$H_2 + H$	$\rightarrow$	$H + H + H$	3.65×10^{-16}	0.0	24300	4.478	T_h	T_h
20	$H + e$	$\rightarrow$	$H^+ + H + e$	6.5×10^{3}	-3.78	159000	13.598	T_e	T_e
21	$H_2^+ + H_2 + e$	$\rightarrow$	$H_2 + H_2$	6.07×10^{-34}	-2.5	0	-15.426	T_e	T_h
22	$H_2^+ + H + e$	$\rightarrow$	$H_2 + H$	6.07×10^{-34}	-2.5	0	-13.598	T_e	T_h
23	$H_2^+ + H + e$	$\rightarrow$	$H + H_2$	1.66×10^{-35}	-2.5	0	-15.426	T_e	T_h
24	$H^+ + H + e$	$\rightarrow$	$H + H$	1.66×10^{-35}	-2.5	0	-13.598	T_e	T_h
25	$NH_3 + M$	$\rightarrow$	$H + NH_2 + M$	3.65×10^{-14}	0.0	47023	4.645	T_h	T_h
26	$NH_3 + M$	$\rightarrow$	$H_2 + NH + M$	1.05×10^{-15}	0.0	47023	4.305	T_h	T_h
27	$NH_3 + NH$	$\rightarrow$	$NH_2 + NH_2$	5.25×10^{-16}	0.0	13508	0.507	T_h	T_h
28	$H + NH_2$	$\rightarrow$	$H_2 + NH$	1.05×10^{-16}	0.0	4456	-0.340	T_h	T_h
29	$NH_2 + M$	$\rightarrow$	$H + NH + M$	1.99×10^{-15}	0.0	38218	4.138	T_h	T_h
30	$NH_2 + N$	$\rightarrow$	$NH + NH$	2.99×10^{-19}	0.0	7602	0.9219	T_h	T_h
31	$H_2 + NH$	$\rightarrow$	$H + NH_2$	1.69×10^{5}	0.0	0	-1.262	T_h	T_h
32	$NH + M$	$\rightarrow$	$H + N + M$	2.99×10^{-16}	0.0	37619	3.2165	T_h	T_h
33	$NH + NH$	$\rightarrow$	$N_2 + H + H$	1.16×10^{-15}	0.0	0	-3.326	T_h	T_h

*Reaction rate α^f can be written by $\alpha^\mathrm{f} = aT^b \exp(-c/T)$ where T is a dependent-temperature.

'M' means all the heavy particles considered.

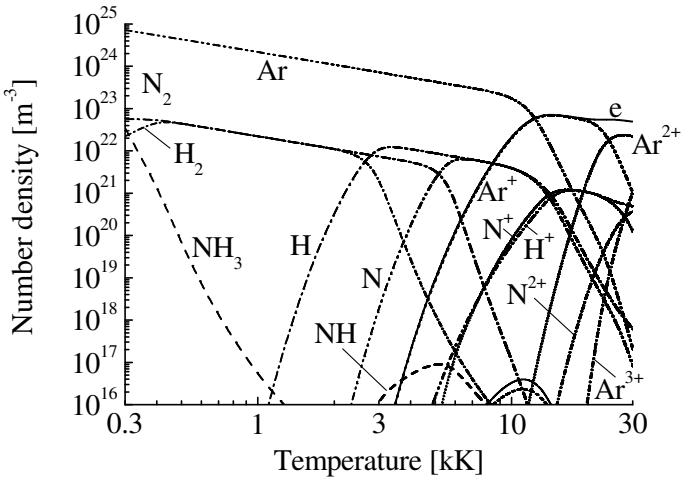

Figure 1: Equilibrium composition of 98%Ar-1%N_2-1%H_2 plasma.

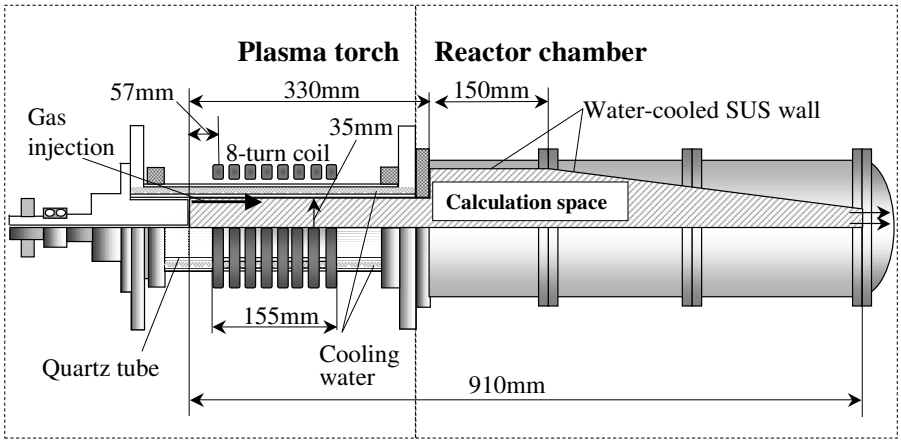

Figure 2: Plasma torch configuration and calculation space.

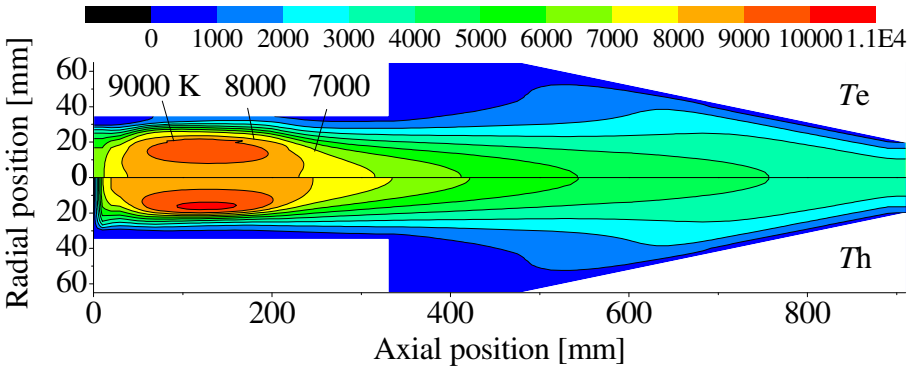

Figure 3: Temperature distribution of 98%Ar-1%N_2-1%H_2 thermal plasma calculated by 2T-NCE model.

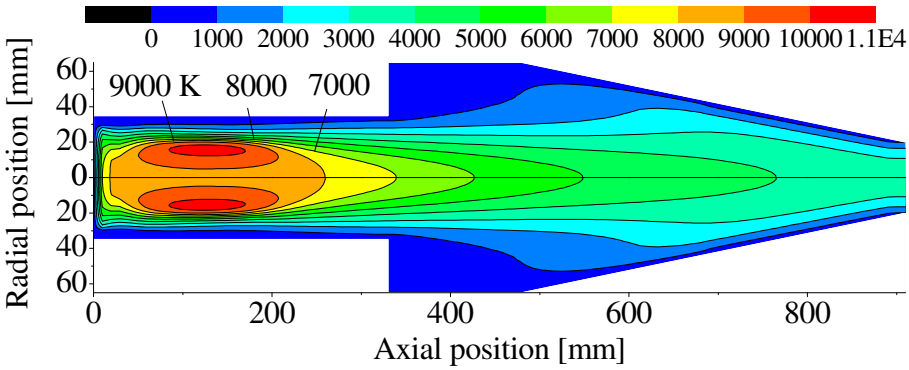

Figure 4: Temperature distribution of 98%Ar-1%N_2-1%H_2 thermal plasma calculated by 1T-CE model.

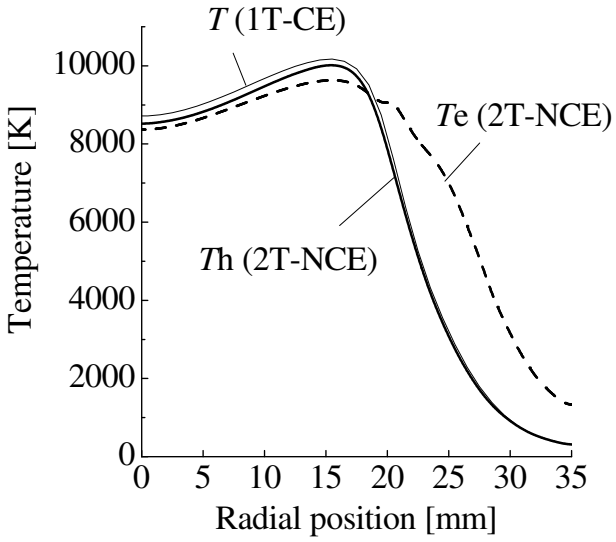

Figure 5: Radial distributions of electron temperature and heavy particle temperature at axial position of 155 mm in 98%Ar-1%N_2-1%H_2 thermal plasma by 2T-NCE model and 1T-CE model.

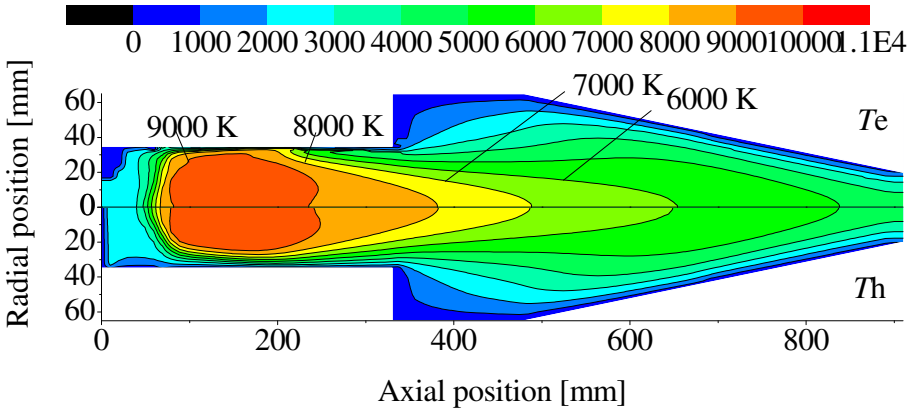

Figure 6: Temperature distributions of 98%Ar-2%N_2 thermal plasma by the 2T-NCE model.

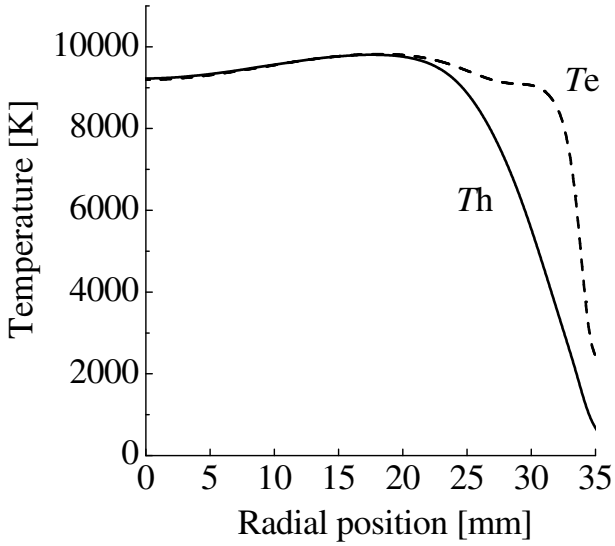

Figure 7: Radial distributions of electron temperature and heavy particle temperature at axial position of 155 mm in 98%Ar-2%N_2 thermal plasma predicted by 2T-NCE model.

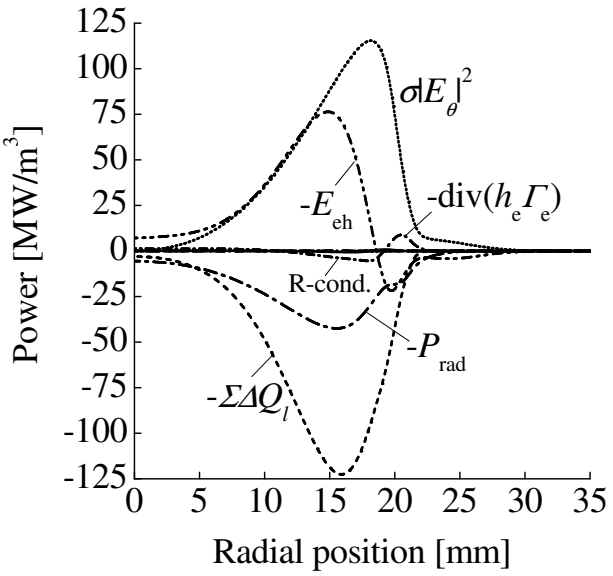

Figure 8: Energy balance for electrons at axial position of 155 mm in 98%Ar-1%N_2-1%H_2 thermal plasma.

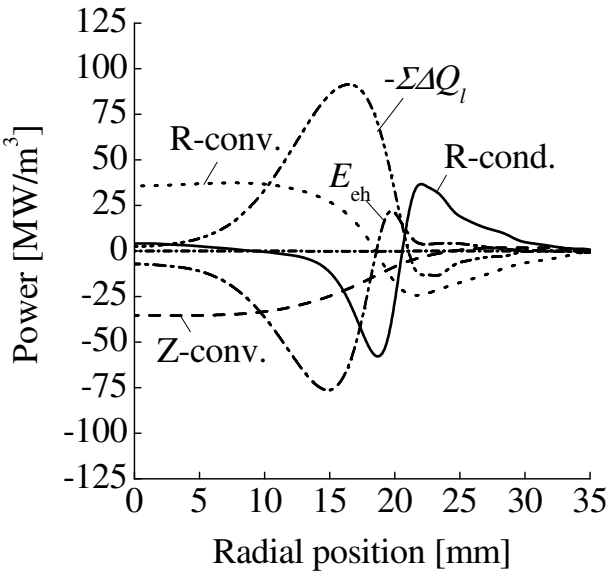

Figure 9: Energy balance for heavy particles at axial position of 155 mm in 98%Ar-1%N_2-1%H_2 thermal plasma.

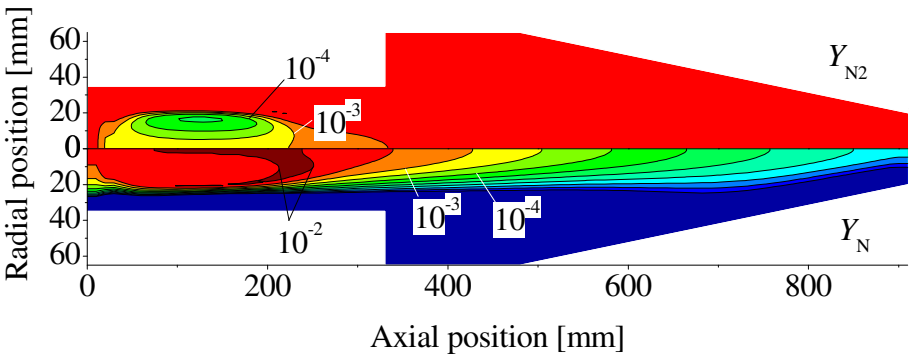

Figure 10: Mass fraction distributions of N_2 and N in 98%Ar-1%N_2-1%H_2 thermal plasma calculated by the 2T-NCE model.

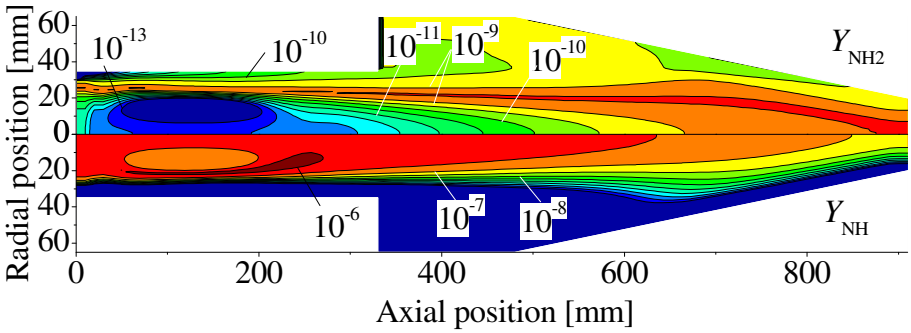

Figure 11: Mass fraction distributions of NH_2 and NH in 98%Ar-1%N_2-1%H_2 thermal plasma by the 2T-NCE model.

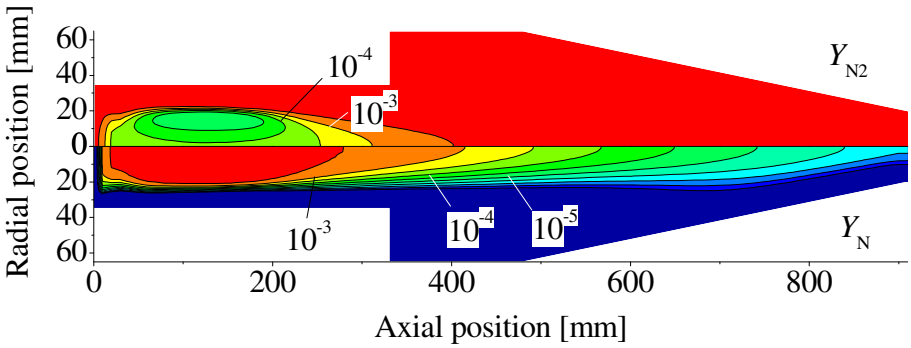

Figure 12: Mass fraction distributions of N_2 and N in 98%Ar-1%N_2-1%H_2 thermal plasma by 1T-CE model.

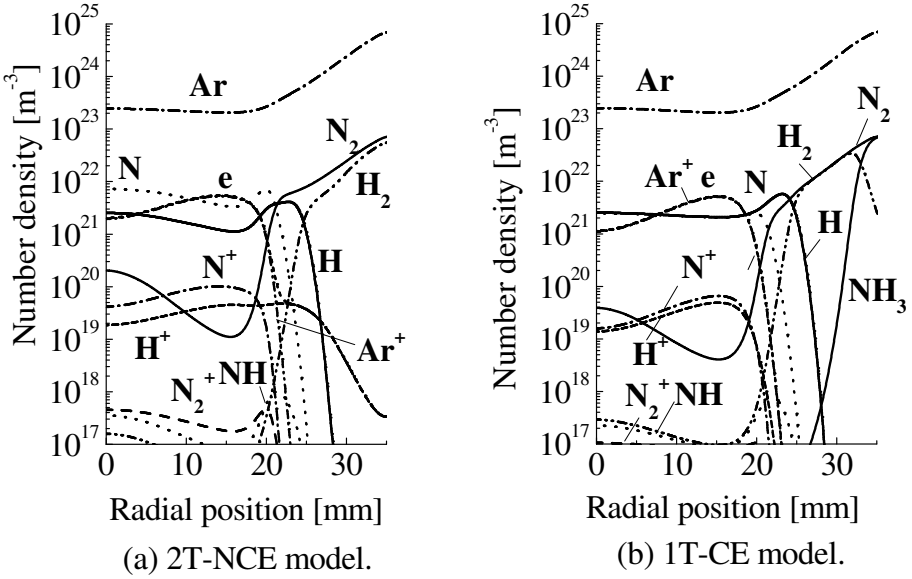

Figure 13: Radial distribution of particle composition at an axial position of 155 mm in 98%Ar-1%N_2-1%H_2 thermal plasma by 2T-NCE and 1T-CE models.